

Coarse-graining MARTINI model for molecular-dynamics simulations of the wetting properties of graphitic surfaces with non-ionic, long-chain and T-shaped surfactants

Danilo Sergi, Giulio Scocchi, and Alberto Ortona

University of Applied Sciences (SUPSI), The iCIMS Research Institute, Galleria 2, CH-6928 Manno, Switzerland

(Dated: November 2, 2018)

We report on a molecular dynamics investigation of the wetting properties of graphitic surfaces by various solutions at concentrations 1 – 8 wt% of commercially available non-ionic surfactants with long hydrophilic chains, linear or T-shaped. These are surfactants of length up to 160 [Å]. It turns out that molecular dynamics simulations of such systems ask for a number of solvent particles that can be reached without seriously compromising computational efficiency only by employing a coarse-grained model. The MARTINI force field with polarizable water offers a framework particularly suited for the parameterization of our systems. In general, its advantages over other coarse-grained models are the possibility to explore faster long time scales and the wider range of applicability. Although the accuracy is sometimes put under question, the results for the wetting properties by pure water are in good agreement with those for the corresponding atomistic systems and theoretical predictions. On the other hand, the bulk properties of various aqueous surfactant solutions indicate that the micellar formation process is too strong. For this reason, a typical experimental configuration is better approached by preparing the droplets with the surfactants arranged in the initial state in the vicinity of contact line. Cross-comparisons are possible and illuminating, but equilibrium contact angles as obtained from simulations overestimate the experimental results. Nevertheless, our findings can provide guidelines for the preliminary assessment and screening of surfactants. Most importantly, it is found that the wetting properties mainly depend on the length and apolarity of the hydrophobic tail, for linear surfactants, and the length of the hydrophilic head-group for T-shaped surfactants. Moreover, the T-shaped topology appears to favor the adsorption of surfactants onto the graphitic surface and faster spreading.

PACS numbers: 47.11.Mn,47.55.dk,47.55.dr,47.55.np

I. INTRODUCTION

Molecular dynamics (MD) simulations have become an important complement to experimental and theoretical work across a variety of disciplines. Often, one of the encountered obstacles to further advances are the prohibitive computational resources necessary for a description at the molecular level of systems containing a large number of particles [1]. This situation is in general quite common when water is involved as solvent. One way to overcome this limitation is to reduce the degrees of freedom to the essential for the issues under investigation. This procedure is referred to as coarse-graining because the system is suitably organized into units identifying groups of atoms. To achieve this, two schemes are basically available [2–5]. The differences mainly reside in the decomposition of the system into building blocks and the selected properties according to which inter-particle interactions are calibrated. Our work is based on the MARTINI force field because allowing to build readily and systematically systems of coarse-grained (CG) units in a prescribed way [2]. Within this framework four heavy atoms are generally mapped into one interaction site. The resulting beads are classified into four main categories that separate further into subtypes. Lennard-Jones (LJ) interactions are organized into ten levels of strength and evaluated with a function of type 12-6. In its original formulation, the MARTINI model does not contemplate solid phases [2]. Following empirical arguments, we treat graphitic surfaces and their wetting properties by surfactant solutions. In that respect, the surface tension of water is of course a key property. The polarizable MARTINI model for water [3] still underestimates the experimental

value. The expected balance of forces at the interface with the graphitic surface is approximately restored by tuning the interaction strength of the relative LJ potential. In this way, we first reproduce in the macroscopic limit the contact angle for pure water from measurements at present carried out under the most ideal conditions [6]. Interestingly, our results correlate well with those using atomistic models for water consistent with the experimental surface tension [7, 8]. This allows us to conclude that the MARTINI force field can provide an effective framework for investigating the wetting properties of surfaces. Surfactants are molecules exhibiting opposite behavior toward water at their extremes, namely hydrophilic in the headgroup and hydrophobic in the tail group. Importantly, these competing attributes are responsible for the decrease of the surface tension of the resulting solution [9]. In practice, this means that an aqueous solution would wet better a surface with the addition of surfactants. At higher concentrations, another important property related to the amphiphilic nature of surfactants is their ability to self-assemble into micelles [9]. Applications in the industry are innumerable, including printing, detergency, oil recovery, dispersion, emulsification, disinfection, etc. [9]. In this work, we concentrate on solutions with non-ionic surfactants. As conveyed by the title, emphasis is put on the wetting properties by measuring the contact angle of droplets. The identity of the surfactants under investigation is confidential for industrial reasons. Specifically, their use as wetting agents is necessary for the optimal dispersion of reinforcement fillers in polymeric matrices (low chemical compatibility to each other) [10]. This phase is rather prominent in the manufacturing route of composite materials in order to meet challenging, target properties [11, 12]. Our work aims at providing useful guidance for planning applications.

So, the basic mechanisms governing wetting phenomena by aqueous surfactant solutions are at the center of our attention. The strategy consists in simulating six representative surfactants differing in simple attributes such as the length of the hydrophilic and hydrophobic groups or the topology (linear and T-shaped). Our research develops as follows. In the next Section, the MARTINI representation of all the constituents of the systems is introduced. Section III is concerned with the general MD simulation settings. In Sec. IV are presented the results for systems of pure water and with surfactants: first the bulk properties of solutions and then the wetting behavior on graphitic surfaces. The last Section is devoted to conclusive remarks.

II. COARSE-GRAINING OF THE SYSTEMS

Force field. The MARTINI force field is designed in order to account for a variety of chemical compounds preventing the need to recalibrate the various interaction parameters for every application [2, 3]. The idea is to classify atomic functional groups into four main categories: polar, nonpolar, apolar and charged. Every category subdivides further into subtypes so as to represent more finely the underlying structural properties. Ten levels of interaction are possible between the diverse types of CG particles. More precisely, inter-particle LJ forces are derived from the potential energy

$$U_{\text{LJ}}(r_{ij}) = 4\epsilon_{ij} \left[\left(\frac{\sigma_{ij}}{r_{ij}} \right)^{12} - \left(\frac{\sigma_{ij}}{r_{ij}} \right)^6 \right].$$

The indices i and j label the particles. r_{ij} is the distance separating pairs of particles. The parameter ϵ_{ij} adjusts the strength of the forces according to the available levels of interaction. The coefficient σ_{ij} is related to the equilibrium distance between particles via the formula $2^{1/6}\sigma_{ij}$. If $r_{ij} < 2^{1/6}\sigma_{ij}$ the force is repulsive, otherwise it is attractive. The parameter σ_{ij} is also usually referred to as molecular diameter. Electrostatic interactions are computed from the coulombic potential

$$U_{\text{C}}(r_{ij}) = \frac{q_i q_j}{4\pi\epsilon_0\epsilon_r r_{ij}}.$$

q_i is the partial charge of the i -th particle; ϵ_0 is the permittivity in vacuum and ϵ_r is the relative dielectric constant. For the standard MARTINI model $\epsilon_r = 15$, while for the polarizable model used here $\epsilon_r = 2.5$. Non-bonded interactions are corrected separately to zero using the shift function [13]

$$S(r_{ij}) = \begin{cases} C & r_{ij} \leq r_{\text{shift}} \\ \frac{A}{3}(r_{ij} - r_{\text{shift}})^3 + \frac{B}{4}(r_{ij} - r_{\text{shift}})^4 + C & r_{\text{shift}} < r_{ij} < r_c, \end{cases}$$

where r_{shift} is the inner cutoff distance and r_c is the outer cutoff distance. The constants A , B and C are determined from boundary conditions. Intra-particle interactions take into account bond and angle interactions. Bonded particles interact via the harmonic potential

$$U_{\text{b}}(r_{ij}) = K_{\text{b}}(r_{ij} - r_0)^2,$$

where r_0 is the equilibrium distance and K_{b} the energy constant. The standard MARTINI values for these parameters are $r_0 = 4.7$ [Å] and $K_{\text{b}} = 1.5$ [kcal/mol/Å²]. Angle interactions are described by the potential

$$U(\theta_{ijk}) = K_{\text{a}}[\cos(\theta_{ijk}) - \cos(\theta_0)]^2.$$

θ_{ijk} is the angle formed by triplets of bonded particles; θ_0 is the equilibrium angle; K_{a} is the coupling constant, for which the standard MARTINI value is $K_{\text{a}} = 3.0$ [kcal/mol].

Water. A CG bead of polarizable MARTINI water [3] consists of three particles W_0 , W_{\pm} of equal mass 24 [g/mol] and of partial charge $q_0 = 0$ [e] and $q_{\pm} = \pm 0.46$ [e], respectively. The charged particles are bonded to the neutral one and the bond length is kept fixed at 1.4 [Å]. The angle degree of freedom is modeled as a harmonic oscillator of elastic constant $K_{\text{a}}^{\text{W}} = 0.5019$ [kcal/mol] and equilibrium angle of 0°. Lennard-Jones forces are considered only among the central particles W_0 with interaction parameters $\epsilon_{\text{WW}} = 0.956$ [kcal/mol] and $\sigma_{\text{WW}} = 4.7$ [Å]. With the charged particles W_{\pm} , the polarization is treated explicitly and the relative dielectric constant is thus set to $\epsilon_r = 2.5$ (cf. Refs. [2, 3]). Furthermore, Coulomb and van der Waals forces among particles belonging to the same water bead are omitted.

Graphene. The graphene is parameterized by placing at the center of every ring of carbon atoms one interaction site. As a consequence, every bead has mass 24 [g/mol] because representing on average two atoms. The interaction parameter ϵ_{CW} between the beads of water (W_0) and graphene is fixed from the wetting properties of pure water. We choose the value of ϵ_{CW} that reproduces the result for the contact angle in the macroscopic limit reported in Ref. [6]. The parameter σ_{CW} is set equal to $\sigma_{\text{CW}} = 6.24$ [Å]. This value yields approximately the equilibrium distance of 7 [Å]. The solid phase is obtained by two parallel planes of CG graphene. The two planes are separated by 3.4 [Å] with the lower one translated by the vector $(l/2, \sqrt{3}l/2)$ with respect to the upper one. Here l is the length of C-C bonds in the all-atom case. This arrangement is intended to reproduce the structure of a graphite crystal.

Surfactants. The atomic structure of the surfactants is reduced according to the guidelines detailed in Ref. [2]. In order to compare our work to previous similar studies [14], we also consider solutions containing the non-ionic surfactant C₈E₄ (tetraethylene glycol octyl ether). We adopt the mappings C₁-C₁-P₅-P₅ and C₁-C₁-Na-Na-P₄ proposed in Ref. [14]. The first representation will be referenced as C₈E₄-P₅ surfactant while the latter as C₈E₄-NaNaP₄ [14]. Both molecules are linear with every equilibrium bond length equal to $r_0 = 4.7$ [Å]; all equilibrium angles are of course $\theta_0 = 180^\circ$. The energy constants are also the standard MARTINI values [2], that is, $K_{\text{b}} = 1.5$ [kcal/mol/Å²] and $K_{\text{a}} = 3.0$ [kcal/mol]. For the mass of the beads, we use in this case $m_{\text{P}_4} = 72$ [g/mol], $m_{\text{Na}} = 56$ [g/mol] and $m_{\text{C}_1} = 56$ [g/mol]. The LJ parameters are readily obtained from Ref. [2] with all equilibrium distances set to 4.7 [Å]. The wetting properties of graphitic surfaces are studied in relation to five non-ionic surfactants, long-chain and T-shaped. The first surfactant will be referred to as L1. Its molecule is linear and it is applied the MARTINI representation (C₁)₃(P₄)₁₀. The mass is again $m_{\text{C}_1} = 56$ [g/mol] for the

tail beads, while we use $m_{P_4} = 44$ [g/mol] for the hydrophilic head. The second surfactant has representation $(C_1)_3(P_4)_{20}$ and will be designated by L2. All topology and interaction parameters are the same as for the surfactant L1. The third linear surfactant L3 is mapped into $(C_1)_4(P_4)_{30}$. All the parameters are the same as for the surfactant L1. Regarding the T-shaped surfactants, we distinguish the T1 and T2 topologies. These surfactants differ by the length of the hydrophilic headgroup. The surfactant T1 has a linear chain made of ten beads P_4 , while the surfactant T2 counts twenty beads P_4 arranged linearly. In both cases, the hydrophobic tail consists of three aligned beads C_1 and in the middle is attached the hydrophilic chain. For the angle C_1 - C_1 - P_4 (vertex in the central bead), the equilibrium value is set to 90° , and the standard potential and interaction parameter of the MARTINI force field [2] are used. All the other parameters are the same as for the linear surfactants. The hydrophobic tail of the surfactant T3 is made of five C_1 beads. At the central bead is attached the linear, hydrophilic head of length twenty P_4 units. All the other settings for T-shaped surfactants apply also in this case.

III. SIMULATIONS

All simulations are performed with the molecular dynamics code LAMMPS [15–17]. Newton’s equations of motion are integrated with the Verlet algorithm using a Nosé-Hoover scheme in the specified ensemble; the timestep size is of 20 [fs]. Non-bonded interactions are cut off at $r_c = 12$ [Å] and computed with the potential lj/gromacs/coul/gromacs [13]. The LJ potential is shifted from $r_{\text{shift}} = 9$ [Å] to r_c , while the electrostatic contribution is shifted from $r_{\text{shift}} = 0$ [Å] to r_c . Long-range interactions are not taken into account. The bond length between W_0 and W_{\pm} particles is maintained rigid with the SHAKE algorithm [18]. Three-body interactions of surfactants are computed with the cosine/squared potential. The neighbor list is rebuilt at most every 5 timesteps. It is not necessary to divide the bond and angle coefficients given here by 2. Then, all simulation times must be meant as actual [3]. Unless specified otherwise, these parameters remain unchanged in the various simulations. The motivations for these settings can be found in Refs. [2, 3].

IV. RESULTS AND DISCUSSION

Bulk properties of CG water. As starting configuration, 1’000 beads of water are arranged with the W_0 particles on the vertices of a simple cubic lattice. The side of the unit cell is 4.5 [Å]. The system is let evolve for 100 [ns] at NPT conditions. The time of evolution is long in order to verify that we do not incur in freezing. The target temperature and pressure are $T = 298$ [K] and $P = 1$ [atm]. The system is studied by recording 1’000 evenly-spaced frames over the course of the last 50 [ns]. Table I lists some average bulk properties of the cubic box of CG water. The W_0 - W_0 radial distribution func-

L [Å]	V [Å ³]	ρ [g/Å ³]	d [molecules/Å ³]
48.858	116’629	1.0255	0.0086

Table I: Average characteristics of the cubic simulation box during the NPT dynamics, side length L and volume V , along with the bulk properties of CG water ρ and d , mass and particle densities respectively.

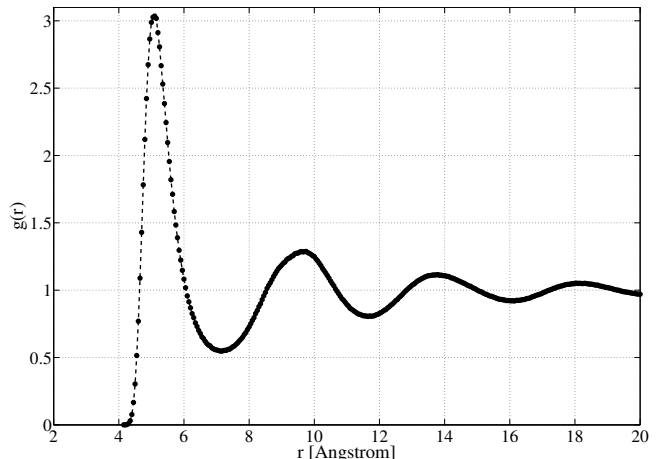


Figure 1: W_0 - W_0 RDF as obtained from the NPT dynamics for the polarizable MARTINI water model.

tion, $g(r)$, is computed by means of the formula

$$\frac{N}{V} g(r) 4\pi r^2 \Delta r = S(r) .$$

N is the number of water beads and V the volume of the simulation domain. $S(r)$ counts the average number of W_0 particles falling in a shell of width $\Delta r = 0.05$ [Å] centered around a given W_0 particle at distance r . The radial distribution function (RDF) is shown in Fig. 1. In general, our results compare well with those of the original work for the present model of CG water [3]. The standard deviation of the volume of the simulation domain is 0.78% of the average value. For this reason, we safely replicate the last configuration of this NPT simulation and extract the assemblies for any subsequent dynamics containing pure CG water.

Spherical droplets. As a matter of calibration of the interaction parameter ϵ_{CW} , droplets of pure CG water spreading on the CG graphene are first considered. The interaction strength ϵ_{CW} is varied in the range 0.04 – 0.08 [kcal/mol]. Every initial configuration is composed by a hemispherical droplet of 17’927 beads centered above the upper-lying plane of graphene at a distance of 7 [Å]. The radius of the hemisphere is 100 [Å]. The planes of graphene are squared with side length 320 [Å]. The boundary conditions are periodic. Every system is evolved in the canonical ensemble for 60 [ns] at $T = 298$ [K]. The systems are studied from 1’000 frames recorded during the last 40 [ns]. These dynamics are shorter because for long times of evolution the droplets systematically exhibit excessive stratification. The onset of this phenomenon

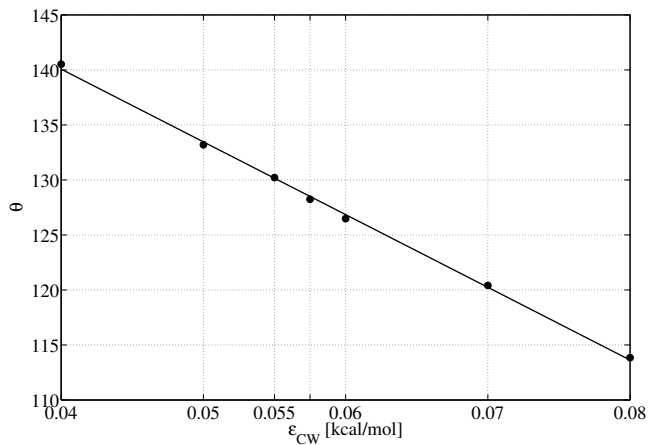


Figure 2: Contact angle as a function of the strength parameter. Matching with the experimental result [6] occurs approximately for $\epsilon_{CW} = 0.0575$ [kcal/mol].

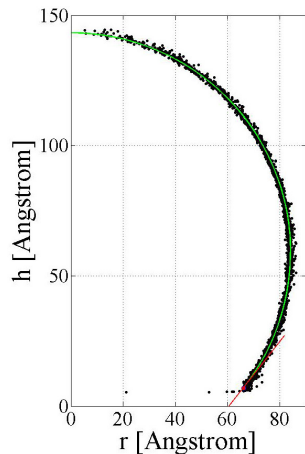


Figure 3: (Color online) Profile of the spherical droplet for $\epsilon_{CW} = 0.0575$ [kcal/mol]. The data are analyzed following the method presented in Refs. [8, 19, 20]. The green line is a fit to the data under the assumption of a spherical shape of the droplet. The tangent at the contact line, where the solid, liquid and vapor phases meet, is in red and the contact angle is measured to be 128.2° .

depends on several parameters, first of all the equilibrium distance of the liquid interface from graphene. Presumably, this shortcoming might be avoided with an involved work of refinement of the force field. We do not insist on this aspect because we expect that the presence of surfactant molecules would reduce the formation of layers of solvent particles. Furthermore, higher temperatures could retard this phenomenon because of faster kinetics. Then, the behavior at room temperature could be extrapolated. For all simulations presented in this Article, stratification never occurred and, as we shall see, our outcomes are still in reasonable agreement with the atomistic results and the general theoretical predictions. Figure 2 shows the dependence of the contact angle on the parameter ϵ_{CW} . These data clearly satisfy a linear relation as in the atomistic case [8]. For $\epsilon_{CW} = 0.0575$ [kcal/mol], it is found

r [Å]	no. water beads	θ [°]
80	25'933	128.0°
90	32'742	128.7°
100	40'430	129.0°
110	48'800	129.9°
120	58'173	130.4°
130	68'255	130.4°

Table II: Contact angle as a function of the initial radius of cylinders. The variations of θ indicate that the macroscopic regime is reached for radii ~ 130 [Å].

T [K]	d [molecules/Å ³]	r_f [Å]	θ [°]
298	0.0076	100.3	130.4°
305	0.0075	101.8	129.3°
310	0.0075	101.1	130.6°
315	0.0075	101.3	130.8°
320	0.0074	101.4	131.4°
350	0.0071	102.0	132.9°
400	0.0065	104.1	136.2°

Table III: Variations from temperature rise for the cylinder of initial radius 130 [Å]: particle density d , final radius r_f and contact angle θ .

a contact angle of 128.2° . This result reproduces the experimental value reported in Ref. [6]. The profile of the droplet in this case is shown in Fig. 3. In principle, other coarse-grained force fields are available for such investigations [4, 5]. For example, in Ref. [21] the wetting properties of pure water on a flat surface were investigated by taking a LJ function of type 6-3 for the interaction between the liquid and solid phases. Using the same CG water, preliminary results indicate that the process of stratification on a molecular graphitic substrate occurs quite fast with the liquid-solid interactions described by a LJ potential of type 12-6. Ultimately, the assessment of other coarse-grained force fields for wetting studies warrants a detailed discussion, which is beyond the scope of the present study.

Cylindrical droplets. We now want to investigate the dependence of the contact angle on size and temperature. To achieve this, six hemicylindrical droplets of radii from 80 to 130 [Å] are considered. The x side of the simulation domain is always 300 [Å], corresponding to the height of every hemicylinder. The y side is always 120 [Å] larger than the diameter of the droplets. In the initial configuration, the droplets are centered in the xy plane. All other simulation settings are the same employed for spherical droplets. In Tab. II are listed the contact angles measured from the profiles of cylinders with increasing radii. The contact angles vary only of a few degrees and thus we conclude that size effects are negligible with radii ~ 130 [Å]. It is interesting to remark that the contact angle for cylinders is slightly larger than that for the spherical droplet, as observed for atomistic systems approaching the macroscopic regime [8]. For the largest cylinder, different temperatures are considered. The results of Tab. III suggests that variations

over a range of 100 [K] have no drastic effect. The results reported here for the temperature dependence of contact angle are in line with those for atomistic systems [7]. In the following, cylindrical droplets are preferred to spherical ones because the simulations turn out to be accelerated [22]. More precisely, the CPU timings for the cylindrical droplet of radius 80 [Å] are comparable with those of spherical droplets, of radius 100 [Å]. The former system contains 25'933 water beads while the latter 17'927. The reason for the speed-up is that parallelization based on spatial decomposition [17] is more efficient for cylinders because the projection of the particles on the xy plane of the simulation domain gives a better coverage.

Bulk properties of surfactant solutions. Here we consider boxes of CG water containing surfactants. In the initial configuration, the surfactant molecules are arranged regularly between two slabs of water. Every simulation lasted for 300 [ns] at NPT conditions. The target pressure is always 1 [atm] while the temperature is adjusted to different values. Data for analysis are recorded every 5 [ns]. To start with, we want to compare the predictions of the MARTINI model with polarizable water [3] to those of the standard version [2]. To this end, we first simulate 175 surfactant molecules of C_8E_4 -NaNaP₄ with 18'339 water beads, as done in Ref. [14]. This concentration leads to the formation of micelles [14]. We look at the RDF between C_1 beads belonging to different surfactant molecules in order to extract the equilibrium distance between tail beads in the same micelle. From Fig. 4, we see that there is a first peak around 5.1 [Å], while the first minimum occurs at about $r_{\min} = 7$ [Å]. As a consequence, we shall assume that the surfactants with all of their C_1 beads separated by more than r_{\min} are free with respect to each other. The first pronounced peak, together with the fact that the RDF tends to zero, indicate that the tail beads are confined in relatively small regions of the whole simulation domain. Indeed, for all temperatures it is found that most of the surfactant molecules cluster into micelles, corroborating the results reported in Ref. [14]. Table IV lists basic statistical indicators relative to the size distribution of micelles. As the temperature increases, the average size of micelles increases and there is clearly more dispersion around the mean value (enhanced polydispersity). Furthermore, the size of micelles (aggregation number) tends to increase with temperature, as expected for non-ionic surfactants [23]. In that respect, it is interesting to remark that the first peak of the C_1 - C_1 (tail beads) RDF is more marked at higher temperatures (see Fig. 4). For the other representation of the surfactant C_8E_4 [14] (see Sec. II), we also consider 175 molecules with 18'339 water beads at the temperature of 350 [K]. The C_1 - C_1 RDF for the surfactant C_8E_4 -P₅ is similar to those of Fig. 4 and the characteristic distance r_{\min} associated with micelle formation is 7 [Å] also in this case. For this mapping, the headgroup is more polar and the process of micelle formation is effectively weakened. Figure 5 shows the number of free surfactants in the course of time. Table IV presents some statistics for micelles. The critical micelle concentration (CMC) is the concentration at which micelles start forming. We calculate the CMC from the average number of free surfactants [14]. In this way, it is understood that the removal of

micelles leaves the surfactant solution at CMC. After 300 [ns] of dynamics there remain five free surfactant molecules (see Fig. 5 and Tab. IV): it is thus predicted a CMC of 4.4×10^{-3} [M]. Now, the CMCs at two different temperatures T_1 and T_2 are related by $CMC(T_2) = [CMC(T_1)]^{T_1/T_2}$ [14, 24]. From the experimental value $CMC(T_1 = 298[K]) = 8 \times 10^{-3}$ [M] [25, 26] it is obtained a CMC of 16×10^{-3} at 350 [K]. It turns out that our result underestimates this value but is closer than the finding within the standard MARTINI model of 35×10^{-3} [M] [14]. For the surfactant L2, L3, T1 and T2, we apply the same simulation settings with the exception that the timestep size is reduced to 10 [fs] for stability reasons related to bond interactions of the surfactant molecules. The temperature is always kept fixed at $T = 298$ [K] and the initial state consists of a given number of surfactant molecules, for the concentrations of Tab. V, between two slabs of water beads (50'000 in total). For the typical experimental concentration of 1 wt%, the RDFs of Fig. 6 indicate that the tail beads, for the surfactant L2, are separated by larger distances because the first maximum is lower. From the size distributions of micelles plotted in Fig. 7, it can be seen that the linear surfactants tend to form larger micelles on average. A summary of micelle statistics is given in Tab. V; in all cases we used $r_{\min} = 7$ [Å] (cf. Fig. 6).

Wetting with surfactants. Also for this train of simulations, the timestep size is reduced to 10 [fs]. In all other respects, the settings used for cylindrical droplets of pure water are maintained. The effect of the presence of surfactants is to lower the contact angle and this is possible if the tail beads, displaying hydrophobic behavior, interact more strongly with the CG graphene than the head beads P₄. For this reason, it is assumed that the interaction strength is $2 \times \epsilon_{CW} = 0.115$ [kcal/mol]. This approach is chemically consistent since, in graphene, carbon atoms have no polarity. The parameter σ for the LJ interactions with graphene beads is again 6.24 [Å]. The results of Tab. VI indicate that the contact angle is almost insensitive to significant variations of surfactant concentration using equilibrated solutions. Since in general it is observed a stronger micellization process, we repeat the previous simulations with cylindrical droplets of pure water and the surfactants arranged between water and graphene as illustrated in Fig. 8. In this way, the solution is not yet properly equilibrated, but more surfactant molecules are closer to the expected configuration, that is, near the contact line [22, 27, 28]. At 1 wt%, all the systems still do not experience any influence of the presence of surfactants (see Tab. VII). It is worth noting that, in similar studies [29, 30], low surfactant concentrations resulted in a transient increase of the surface tension for the MARTINI model. On the other hand, the concentration around 4 wt% provides a basis of comparison among the different systems. The results for linear surfactants prove that, in first approximation, the dominant factors promoting wetting are the length and apolarity of the hydrophobic tail. Indeed, comparison between surfactants L2 and L3 indicate that one single C_1 bead is sufficient to counteract the effect of ten P₄ beads (their contact angles differ by a few degrees). We want to highlight the preferred arrangement of surfactant molecules inside the droplets. To this end, it is useful to look at the spa-

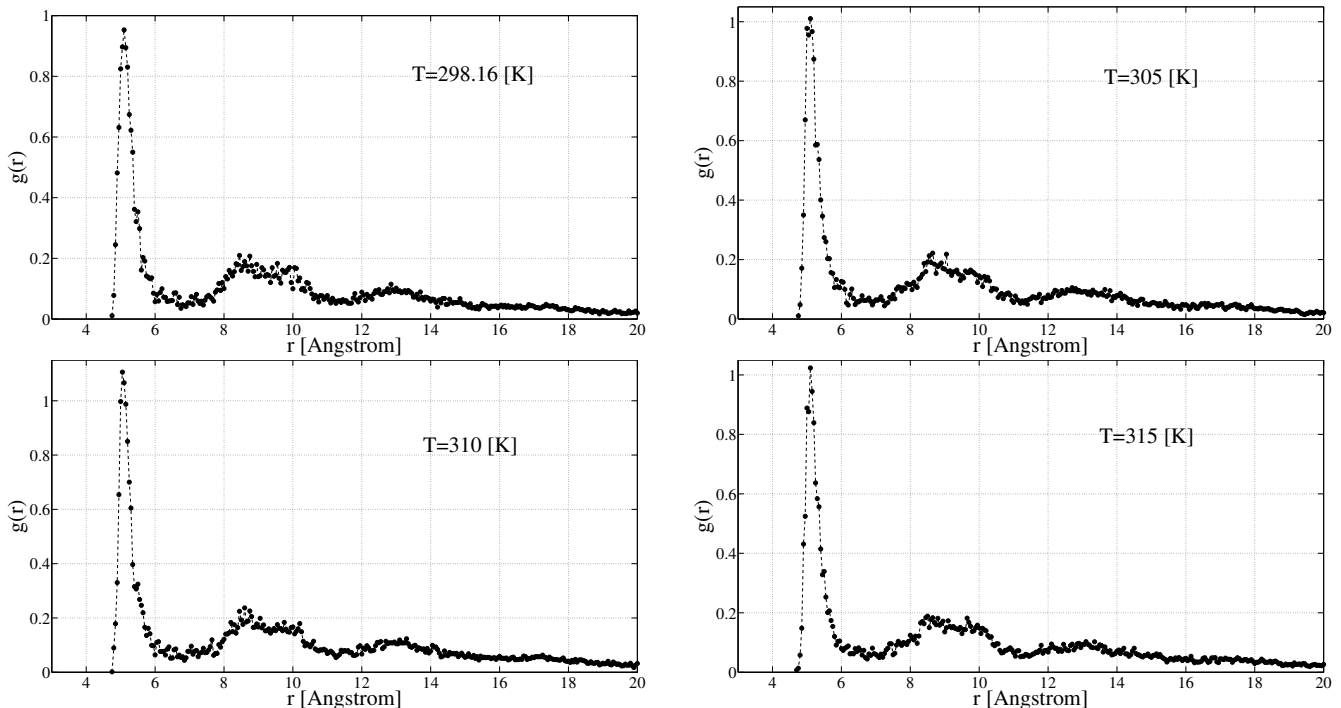


Figure 4: RDFs relative to the tail beads C_1 of the surfactant C_8E_4 - $NaNaP_4$ from isobaric-isothermal dynamics. Average is taken over the last 100 [ns] of the whole evolution.

Mapping	T [K]	Volume [\AA^3]	C [M]	Average	Variance	Size range	no. monomers	CMC [M]
C_8E_4 - $NaNaP_4$	298	1'845'116	0.158	17.5	81.8	5-38	0.0	—
	305	1'846'956	0.158	25.0	244.9	7-53	0.0	—
	310	1'847'152	0.158	25.0	150.1	8-42	0.0	—
	315	1'847'130	0.158	25.0	305.0	11-63	0.0	—
C_8E_4 - P_5	350	1'879'769	0.154	6.0	21.1	1-18	5.0	4.4×10^{-3}

Table IV: Micelle size statistics over the last 100 [ns] for the simulations of surfactant C_8E_4 . With volume we intend the average value of the simulation domain; its standard deviation is always below 0.1%. The symbol C designates the concentration.

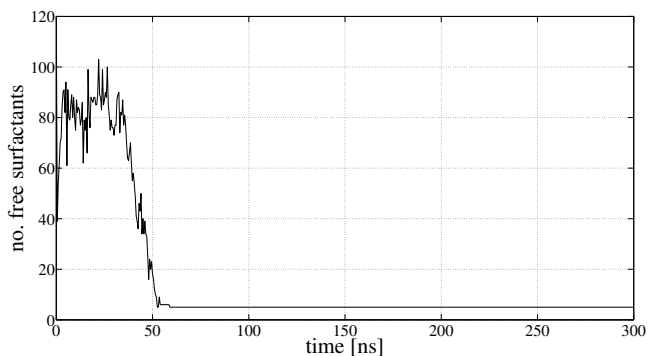


Figure 5: Evolution of the number of free surfactants for the C_8E_4 - P_5 solution at 350 [K] (see Tab. IV).

tial distributions $P_y(y - y_{CM})$ and $P_z(z)$ for C_1 beads along the y and z axes, as the notation suggests. Here y_{CM} is the coordinate of the center of mass of CG water. As evidenced by

Fig. 9, linear surfactant molecules are principally located at the solid-liquid interface. Their organization is not uniform, as indicated by the statistics for micelles of Tab. VII. The weak tendency to form layers, together with the fact that the distribution P_y is strongly peaked around the contact line, give further support to the hypothesis that the number of hydrophobic units is the dominant factor for enhanced wetting. Regarding the T-shaped topology, from Fig. 10 it is seen that less surfactant molecules accumulate along the contact line. The fact that the contact angle remains almost unchanged, as compared to the linear counterparts (see Tab. VII), let us conclude that their action is more effective. In macroscopic systems, they should thus wet better than linear surfactants, since the plateau in Fig. 10 is already almost at the same height of the peaks near the contact line. Interestingly, a longer hydrophobic tail does not lead to a lower contact angle. It thus arises that for T-shaped surfactants a shorter hydrophilic headgroup can enhance wetting more than a longer tail. The plots of Fig. 11 shows that one advantage of the T-shaped topology is

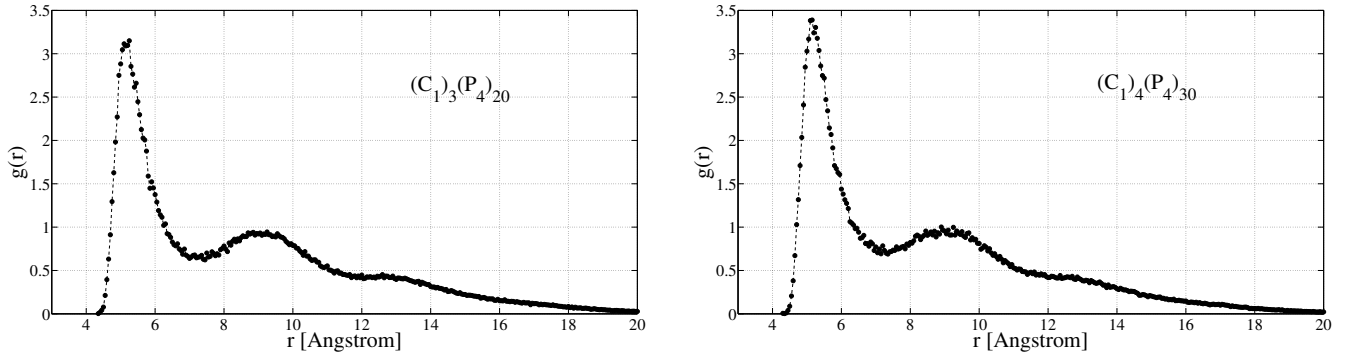


Figure 6: C_1 - C_1 RDFs for the boxes with linear surfactants at 1 wt%; Left: surfactant L2; Right: surfactant L3. Similar results are obtained for the other equilibrated boxes with higher concentrations of surfactant molecules (cf. Tab. V).

Surfactant	Mapping	Volume [\AA^3]	no. surfactants	C [M] - [wt%]	Average	Variance	Size range	no. monomers	CMC [M]
L2	$(C_1)_3(P_4)_{20}$	5'825'561	34	9.7×10^{-3} - 1.0%	6.2	26.0	1-14	1.7	4.8×10^{-4}
		6'503'837	288	7.4×10^{-2} - 8.4%	11.5	54.9	1-85	1.0	2.6×10^{-4}
L3	$(C_1)_4(P_4)_{30}$	5'829'183	24	6.8×10^{-3} - 1.0%	7.4	6.9	2-11	0.0	—
		6'386'342	194	5.0×10^{-2} - 8.3%	15.3	133.7	2-70	0.0	—
T1	$(C_1)_3(P_4)_{10}$	6'506'929	520	1.3×10^{-1} - 8.9%	11.1	54.8	1-50	3.9	1.0×10^{-3}
T2	$(C_1)_3(P_4)_{20}$	6'487'350	288	7.4×10^{-2} - 8.4%	9.3	41.7	1-39	4.2	1.1×10^{-3}

Table V: Basic statistics regarding micelle size for the equilibration of CG water with surfactants at different concentrations. In all cases, the standard deviation of the volume is always around 1% of the average value. C stands for concentration.

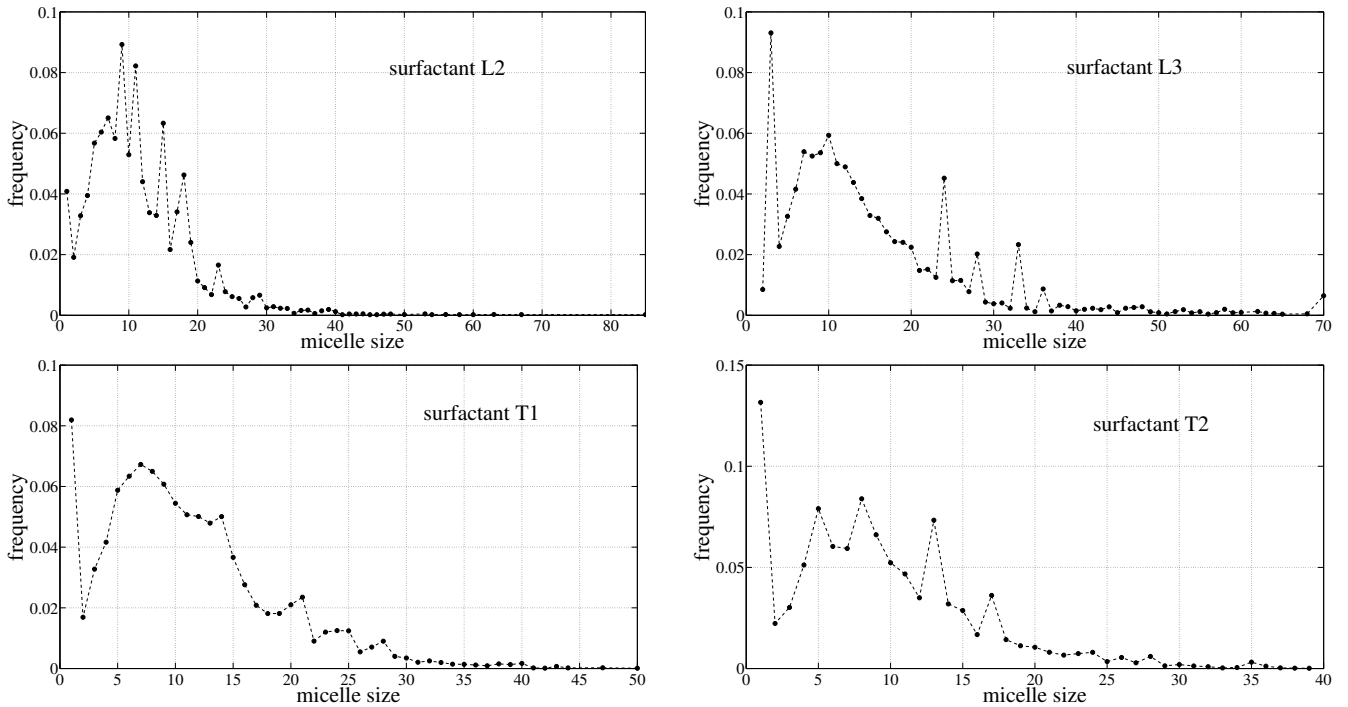


Figure 7: Micelle size distributions as resulting from the simulations of equilibration for two long-chain, linear surfactants and the T-shaped surfactants at 8 wt% concentration. Top: For the L2 surfactant the distribution is peaked around the size of 10, while for the longer surfactant L3 the more frequent micelle is of size 3. Bottom: T-shaped surfactants have less micelle aggregates composed of fifteen or more surfactants. This occurrence has probability 0.26 for the surfactant T1 and 0.18 for the surfactant T2. The same probabilities in the linear case are 0.33 and 0.37 for the surfactants L2 and L3, respectively.

Surfactant	Mapping	no. water beads	no. surfactants	C [wt%]	N_{micelle}	Size range	no. monomers	d [molecules/ \AA^3]	θ [$^\circ$]
L2	$(C_1)_3(P_4)_{20}$	68'727	43	0.9%	17.0	1-14	12.1	0.0074	131.1 $^\circ$
		60'351	359	8.7%	108.3	1-52	55.5	0.0065	130.7 $^\circ$
L3	$(C_1)_4(P_4)_{30}$	68'690	28	0.9%	10.3	1-10	6.6	0.0074	131.1 $^\circ$
		63'555	239	8.1%	36.6	1-66	11.3	0.0068	131.2 $^\circ$

Table VI: Characteristics of the cylindrical droplets of initial radius 130 [\AA] containing linear surfactants. C indicates the concentration. The average number of micelles is designated by N_{micelle} . The cutoff distance for the extraction of micelle clusters is 7 [\AA] (see Fig. 6).

Surfactant	Mapping	no. surfactants	C [wt%]	N_{micelle}	Size range	no. monomers	d [molecules/ \AA^3]	θ [$^\circ$]
L1	$(C_1)_3(P_4)_{10}$	85	1.1%	41.8	1-12	21.6	0.0076	129.6 $^\circ$
		424	5.2%	112.4	1-37	46.3	0.0076	118.2 $^\circ$
		847	10.5%	112.3	1-165	40.6	0.0076	114.5 $^\circ$
L2	$(C_1)_3(P_4)_{20}$	39	0.8%	27.4	1-9	19.4	0.0076	130.1 $^\circ$
		196	4.2%	75.1	1-21	35.4	0.0075	123.5 $^\circ$
		393	8.4%	91.1	1-40	33.9	0.0074	111.7 $^\circ$
L3	$(C_1)_4(P_4)_{30}$	26	0.8%	15.1	1-7	8.5	0.0076	130.5 $^\circ$
		132	4.1%	32.1	1-21	6.7	0.0075	125.0 $^\circ$
		265	8.3%	34.3	1-43	3.7	0.0072	114.9 $^\circ$
		530	16.7%	65.0	1-206	28.9	0.0065	124.7 $^\circ$
T1	$(C_1)_3(P_4)_{10}$	85	1.1%	44.4	1-13	24.1	0.0076	129.2 $^\circ$
		424	5.2%	119.1	1-33	45.4	0.0076	116.0 $^\circ$
T2	$(C_1)_3(P_4)_{20}$	39	0.8%	28.3	1-7	21.0	0.0076	129.8 $^\circ$
		196	4.2%	66.3	1-20	23.4	0.0075	122.1 $^\circ$
		393	8.4%	88.3	1-36	22.2	0.0074	108.3 $^\circ$
T3	$(C_1)_5(P_4)_{20}$	212	5.0%	43.8	1-30	9.6	0.0075	125.1 $^\circ$

Table VII: Results for the cylindrical droplets of initial radius 130 [\AA] with the surfactants arranged in the initial configuration in the proximity of contact line; all droplets contain 68'255 water beads. C stands for concentration; N_{micelle} is the average number of micelles, and size range is the aggregation number variation. Micelle clusters are extracted using a cutoff distance of 7 [\AA] for all surfactants (see Fig. 6). The simulations for the systems containing linear surfactants with a concentration higher than 1 wt% lasted for 100 [ns] and the analysis is performed on data collected under the same conditions over the last 40 [ns]. This choice is dictated by the fact that longer evolutions are necessary in order to reach a state near the equilibrium in these cases. The contact angle for the surfactant L3 at 16.7 wt% is not in line with the results for the lower concentrations suggesting that the system is not yet well equilibrated. For these longer dynamics, the stratification of water did not occur.

faster spreading. After 25 [ns] of dynamics, the contact angles for T-shaped surfactants vary at most of 1.7 $^\circ$ (surfactant T2 at 4.2 wt%). In the same evolution period, with the exception of the surfactant L2 at 4.2 wt%, the variations of the contact angle for linear surfactants are more marked: at least of 3.9 $^\circ$ (surfactant L1 at 5.2 wt%) and at most of 19.2 $^\circ$ (surfactant L2 at 8.4 wt%). The influence of the topology for enhanced spreading was already recognized in the literature [22, 27, 28].

V. CONCLUSIONS

Small concentrations of surfactants around 1 wt% can cause significant reductions of the contact angle. As an example, for the surfactant Triton[®] X-100, the surface tension of water of 72.5 [mN/m] decreases linearly with concentration up to 0.03 wt%, when the minimum of 31 [mN/m] is attained; for higher concentrations the surface tension remains of course constant. It turns out that the proper treatment of wetting phenomena

by aqueous surfactant solutions requires conditions of difficult realization by the present computational capabilities. Coarse-grained models allowed us to move one step further toward a more realistic representation of such systems in terms of surfactant concentrations. At the typical experimental concentration of 1 wt%, the coarse-grained MARTINI force field [2, 3] marks no difference between the surfactants investigated here. For higher concentrations there appears that it is possible to discriminate the wetting behavior of the various surfactants. The main instrumental conclusion of our study is that the length and apolarity of the hydrophobic tail determine to a larger extent the wetting behavior for the linear topology. Instead, the length of the hydrophilic headgroup appears to be more relevant for the T-shaped topology. In the framework of our simulations, the T-shaped topology does not lead to a substantial decrease of contact angle vis-a-vis linear surfactants. Lennard-Jones forces are short range and the reduction of the contact angle is essentially driven by the accumulation of surfactants along the contact line. Micelle statistics demon-

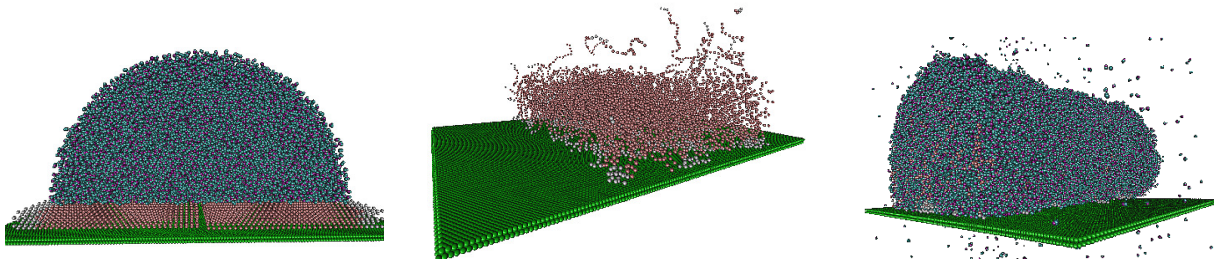


Figure 8: (Color online) From Left to Right: Droplet with surfactant L3 at 8 wt% (see Tab. VII) in the initial configuration, final configuration without water beads and final configuration including water beads. At equilibrium, the surfactant are oriented with their head toward the fluid.

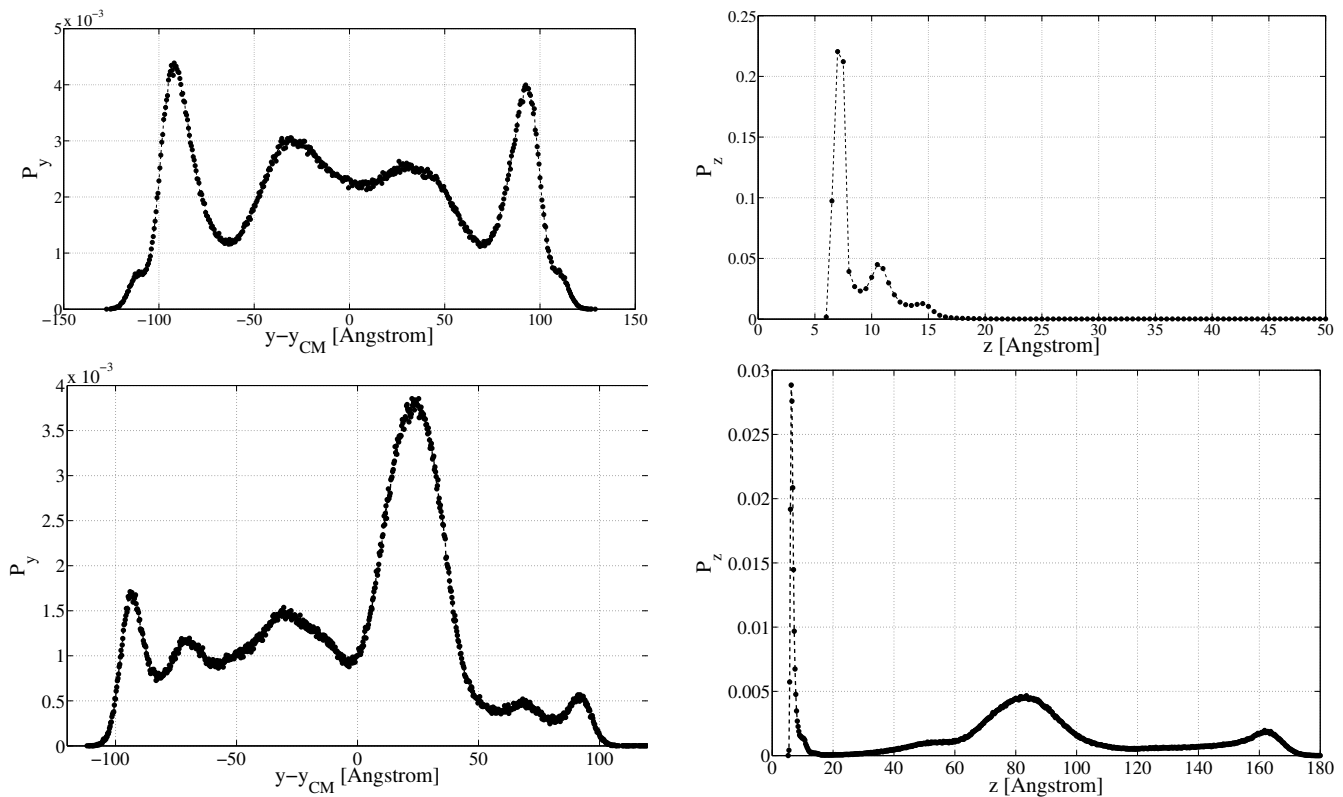


Figure 9: Distributions of C_1 beads in space for the cylindrical droplets containing surfactants L2 at concentration 8 wt%. Top: Results for the droplet prepared as shown in Fig. 8, with the surfactants in the proximity of contact line. Many surfactants are near the contact line, i.e. $|y - y_{CM}| \approx 90$ [Å], and at the solid-liquid interface. Bottom: Results obtained from an equilibrated solution (cf. Tab. VI). The position and height of the peaks indicate that a significant number of surfactants is in the bulk of the droplet. Similar conclusions can be inferred from the outcomes for the other case studies.

strates that linear surfactants pack more tightly, compensating the fact that the hydrophobic tail beads of T-shaped surfactants are on average closer to the graphitic substrate. It thus follows that the stronger self-assembly behavior of surfactants can also favor wetting. On the other hand, the weaker micellization of T-shaped surfactants can result in faster spreading. Finally, our parameterization of surfactants while very simple can encompass and provide benchmarks for several commercially available surfactants. More comparative work remains to be done and our results offer some insight on the complex

interplay between micellization, spreading and wetting.

Acknowledgments

This work was supported by the Swiss Innovation Promotion Agency (KTI/CTI) through BiPCaNP project under grant P. No. 10055.1. Computations were done with the facilities of CSCS and iCIMS-SUPSI. We are grateful to their staff for assistance.

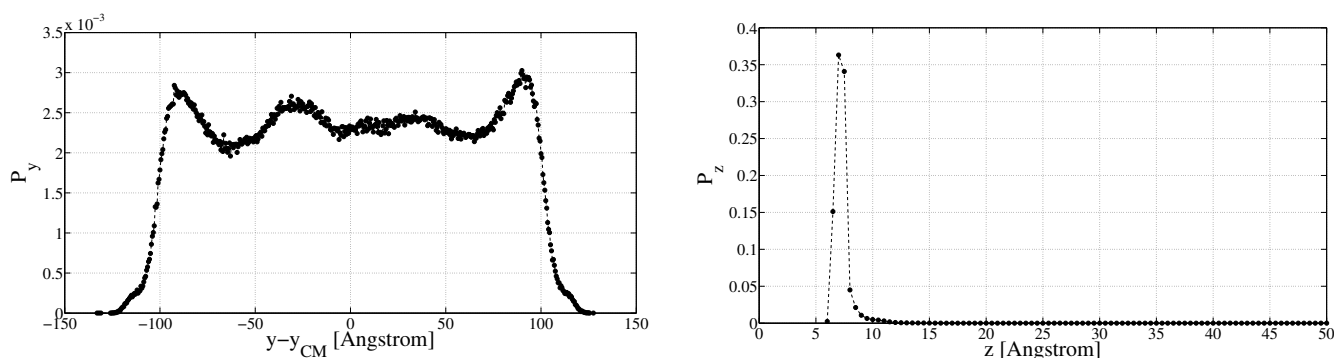


Figure 10: Spatial distributions of C_1 tail beads for the cylindrical droplet containing surfactant T2 at 8 wt% (see Tab. VII). In this case, the surfactants are no longer neatly localized along the contact line. It also appears that the adsorption layer is more uniform (cf. Fig. 9). The plots for the other T-shaped surfactants lead to the same conclusions.

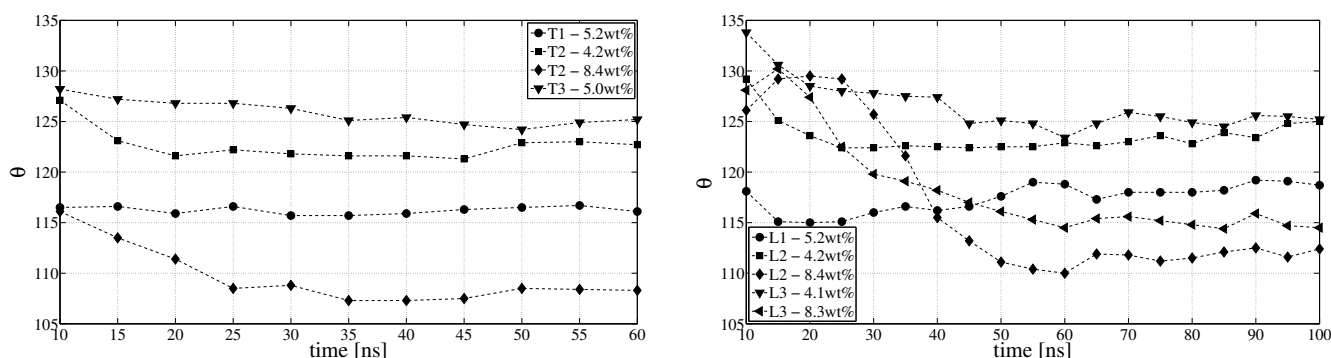


Figure 11: Contact angle θ in the course of time for the cylindrical droplets of Tab. VII. In general, T-shaped surfactants spread faster. The analysis uses the data collected in time intervals of 5 [ns].

-
- [1] M.L. Klein and W. Shinoda, *Science* **321**, 798 (2008).
- [2] S.J. Marrink, H.J. Risselada, S. Yefimov, D.P. Tieleman, A.H. de Vries, *J. Phys. Chem. B* **2007**, 7812 (2007).
- [3] S.O. Yesylevskyy, L.V. Schäfer, D. Sengupta, S. Marrink, *PLoS Comp. Biology* **6**, 1 (2010).
- [4] W. Shinoda, R. DeVane, and M.L. Klein, *Molecular Simulation* **33**, 27 (2007).
- [5] W. Shinoda, R. DeVane, and M.L. Klein, *Soft Matter* **4**, 2454 (2008).
- [6] S. Wang, Y. Zhang, N. Abidi, S. Cabrales, *Langmuir* **25**, 11078 (2009).
- [7] D. Sergi, G. Scocchi and A. Ortona, *Fluid Phase Equilib.* **332**, 173 (2012).
- [8] G. Scocchi, D. Sergi, C. D'Angelo, A. Ortona, *Phys. Rev. E* **84**, 61602 (2011).
- [9] M.J. Rosen, *Surfactants and Interfacial Phenomena* (John Wiley & Sons, New Jersey, 2004).
- [10] L. Vaisman, H.D. Wagner, and G. Marom, *Adv. Colloid Interface Sci.* **128**, 37 (2006).
- [11] E.T. Thostenson, C. Li, and T.-W. Chou, *Compos. Sci. Technol.* **65**, 491 (2005).
- [12] F. Hussain, M. Hojjati, M. Okamoto, R.E. Gorga, *J. Compos. Mater.* **40**, 1511 (2006).
- [13] S.J. Marrink, A.H. de Vries, and A.E. Mark, *J. Chem. Phys. B* **108**, 750 (2004).
- [14] S.A. Sanders and A.Z. Panagiotopoulos, *J. Chem. Phys.* **132**, 114902 (2010).
- [15] S.J. Plimpton, R. Pollock, and M. Stevens, in *Proc. of Eighth SIAM Conf. on Parallel Processing for Scientific Computing*, Minneapolis, MN, March (1997).
- [16] Available at <http://www.cs.sandia.gov/sjplimp/lammps.html>
- [17] S. Plimpton, *J. Comp. Phys.* **117**, 1 (1995).
- [18] J.P. Ryckaert, G. Ciccotti, and H.J.C. Berendsen, *J. Comput. Phys.* **23**, 327 (1977).
- [19] M.J. de Reijter, T.D. Blake, and J. De Coninck, *Langmuir* **15**, 7836 (1999).
- [20] T. Werder, J.H. Walther, R.L. Jaffe, T. Halicioglu, P. Koumoutsakos, *J. Phys. Chem. B* **107**, 1345 (2003).
- [21] U.O.M. Vázquez, W. Shinoda, P.B. Moore, C.-C. Chiu, S.O. Nielsen, *J. Math. Chem.* **45**, 161 (2009).
- [22] J.D. Halverson, C. Maldarelli, A. Couzis, J. Koplik, *Chemical Engineering Science* **64**, 4657 (2009).
- [23] D. Myers, *Surfactant Science and Technology* (John Wiley & Sons, New Jersey, 2006).
- [24] J.N. Israelachvili, D.J. Mitchell, and D.W. Ninham, *J. Chem. Soc., Faraday Trans. 2* **72**, 1525 (1976).
- [25] M. Frindi, B. Michels, and R. Zana, *J. Phys. Chem.* **96**, 6095 (1992).
- [26] T. Telgmann and U. Kaatze, *J. Phys. Chem. A* **104**, 4846 (2000).
- [27] N. Kumar, A. Couzis, and C. Maldarelli, *J. Colloid. Interface*

- Sci. **267**, 272 (2003).
- [28] Y. Shen, A. Couzis, J. Koplik, C. Maldarelli, M.S. Tomassone, Langmuir **21**, 12160 (2005).
- [29] S. Baoukina, L. Monticelli, S.J. Marrink, D.P. Tieleman, Langmuir **23**, 12617 (2007).
- [30] W. Shinoda, R. DeVane, and M.L. Klein, J. Phys. Chem. B **114**, 6836 (2010).